Thiophene Rings Improve the Device Performance of Conjugated Polymers in Polymer Solar Cells with Thick Active Layers

Chunhui Duan, Ke Gao, Fallon J. M. Colberts, Feng Liu, Stefan C. J. Meskers, Martijn M. Wienk, and René A. J. Janssen**

Developing novel materials that tolerate thickness variations of the active layer is critical to further enhance the efficiency of polymer solar cells and enable large-scale manufacturing. Presently, only a few polymers afford high efficiencies at active layer thickness exceeding 200 nm and molecular design guidelines for developing successful materials are lacking. It is thus highly desirable to identify structural factors that determine the performance of semiconducting conjugated polymers in thick-film polymer solar cells. Here, it is demonstrated that thiophene rings, introduced in the backbone of alternating donor–acceptor type conjugated polymers, enhance the fill factor and overall efficiency for thick (>200 nm) solar cells. For a series of fluorinated semiconducting polymers derived from electron-rich benzo[1,2-*b*:4,5-*b*′]-dithiophene units and electron-deficient 5,6-difluorobenzo[2,1,3]thiazole units a steady increase of the fill factor and power conversion efficiency is found when introducing thiophene rings between the donor and acceptor units. The increased performance is a synergistic result of an enhanced hole mobility and a suppressed bimolecular charge recombination, which is attributed to more favorable polymer chain packing and finer phase separation.

1. Introduction

In the past two decades polymer solar cells (PSCs) have attracted considerable attention as a promising next-generation renewable energy conversion technology.[1] The core component of a PSC is the so-called bulk-heterojunction (BHJ) active layer which often consists of a semiconducting polymer and a fullerene derivative to serve as electron donor (hole transporter) and electron acceptor (electron transporter), respectively. Tremendous progress has led to power conversion efficiencies (PCEs) exceeding 11% in both single-junction and multijunction devices benefitting from the creation of state-of-the-art semiconducting polymers, significant improvements in morphology control, interface modification, and device engineering.[2] Moreover, stability tests, which suggest that operational lifetimes approaching ten years are achievable, enhance the prospective of PSCs to become a useful photovoltaic technology.[3] However, the efficiencies of PSCs achieved on a laboratory scale have not yet been successfully translated to the large-area modules that are compatible with high-speed manufacturing such as roll-to-roll processing and ink-jet printing. One of the main reasons is that the device performance usually drops drastically upon increasing the thickness of the active layer. The use of thin (≈100 nm) active layers in PSCs optimized on a laboratory scale significantly restricts the product yield and reproducibility in high-speed manufacturing.[4] Furthermore, a low sensitivity to variations in the thickness of the active layer is also very much in demand for multijunction devices because it allows balancing the performance of subcells in terms of current generation.[5] However, at present most PSCs only perform well in a very narrow thickness range of the active layer, which is usually 80–120 nm.[6]

The often observed reduction in PCEs of PSCs upon increasing the layer thickness mainly results from the sharp drop in fill factor (FF) which outweighs the fact that the increased thickness allows to absorb more incident light and can theoretically afford a higher short-circuit current density (J_{sc}). The loss in FF in thick-film devices is often a result of enhanced bimolecular charge recombination, caused by the increased distance over which charges must be transported and

Dr. C. Duan, F. J. M. Colberts, Dr. S. C. J. Meskers, Dr. M. M. Wienk, Prof. R. A. J. Janssen
Molecular Materials and Nanosystems
Institute for Complex Molecular Systems
Eindhoven University of Technology
P. O. Box 513 5600, MB Eindhoven, The Netherlands
E-mail: r.a.j.janssen@tue.nl

K. Gao, Prof. F. Liu
Department of Physics and Astronomy
and Collaborative Innovation Center of IFSA (CICIFSA)
Shanghai Jiaotong University
Shanghai 200240, P. R. China
E-mail: fengliu82@sjtu.edu.cn

Dr. M. M. Wienk, Prof. R. A. J. Janssen
Dutch Institute for Fundamental Energy Research
De Zaale, 20 5612 AJ, Eindhoven, The Netherlands

The ORCID identification number(s) for the author(s) of this article can be found under https://doi.org/10.1002/aenm.201700519.

DOI: 10.1002/aenm.201700519

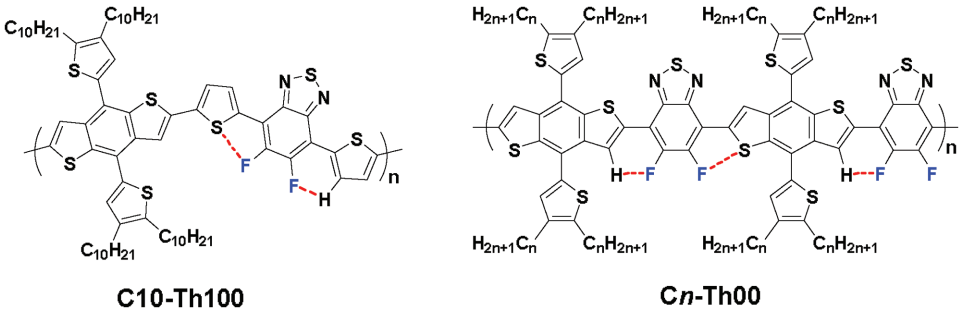

Scheme 1. Chemical structure of C10-Th100 and C*n*-Th00 with possible noncolvalent interactions highlighted in red.

the build-up of space charge in consequence of the reduced internal electric field. Furthermore, low hole mobility and imbalanced hole/electron transport across the active layer also promote bimolecular recombination.[7] Although large numbers of new semiconducting photovoltaic polymers have been reported in the past years, only a few provide FFs over 0.6 and PCEs over 7% at active layer thickness exceeding 200 nm.[5b,8] In Table S1 (Supporting Information) we made an overview for all these successful polymers. Among 32 different polymers, a general observation—without exception—is that they contain thiophene rings in the polymer main chain. We also made an overview for polymers that show PCE ≥8.0% but do not contain thiophene rings in their backbone (Table S2, Supporting Information). It is astonishing that their optimal active layer thicknesses are all around 100 nm, although there are a few reports of efficient thick-film (≥200 nm) PSCs based on these polymers, sometimes via unusual treatments.[9] These observations lead to the question: why are thiophene rings special for efficient thick-film PSCs?

We address this question by investigating a recently developed fluorinated polymer C10-Th100 (denoted previously as BDT-FBT-2T)[5b] and a class of fluorinated polymers C*n*-Th00 (denoted previously as BDT-FBT-C*n*)[10] (**Scheme 1**) based on benzo[1,2-*b*:4,5-*b*′]dithiophene (BDT) and 5,6-difluorobenzo[2,1,3]thiazole (ffBT). The major difference between C10-Th100 and the C*n*-Th00 is the extra thiophene ring in between each BDT and ffBT unit along the conjugated backbone of the polymer. This structural difference results only in minor differences in the optical band gaps and frontier orbital energy levels, but distinctly influences the tolerance to thickness variation of active layer. While C10-Th100 tolerates thickness variations of the active layer from 100 to 250 nm, a similar merit is not observed for the BDT-FBT-C*n* polymers. We note that in both polymers fluorine substitution enables similar noncovalent intrachain interactions (C—H•••F, S•••F, etc.) (Scheme 1). They thus provide an ideal model system to explore the influence of thiophene rings in the main chain of semiconducting polymers on their performance in thick-film PSCs.

In this contribution, we report that in a series of conjugated copolymers based on BDT and ffBT a systematic increase of the number of thiophene rings (**Scheme 2**) results in a monotonically increased FF and PCE in thick (≈250 nm) solar cells. A comprehensive investigation discloses that more favorable polymer chain packing, finer phase separation, enhanced hole mobility, and suppressed bimolecular charge recombination caused by adding more thiophene rings are responsible for the increased FF in thick PSCs. This discovery provides general guidelines for designing practically useful photovoltaic polymers, which will consequently favor large-scale manufacturing of PSCs and multijunction PSCs.

2. Results and Discussion

2.1. Design and Synthesis of Polymers

We developed a family of copolymers C10-Th*x* (Scheme 2), where *x* stands for the percentage of DTffBT monomers and, consequently, 100-*x* corresponds to the percentage of ffBT monomers used in the copolymerization reaction. Varying *x* enables us to systematically investigate the effect of the additional thiophene rings in the main chain on the performance in thick-film solar cells. Notably, we reported several relevant polymers in a recent paper to demonstrate the potential of random copolymers for PSCs.[11] In that paper, another batch of C10-Th100 (denoted previously as Th100) with lower molecular weight was used for a fair comparison, and octyl side chains were applied for the other polymers.[11] In this contribution, decyl side chains were employed for all polymers, and as high molecular weights as possible were pursued for each polymer to make a rigorous investigation.

The C10-Th*x* copolymers were synthesized by the Stille cross-coupling reaction with reasonable yields. Gel permeation chromatography (GPC) measurements performed at 140 °C using *ortho*-dichlorobenzene (*o*-DCB) as the eluent suggest that all polymers possess high molecular weights (**Table 1**; Figure S1, Supporting Information). The number-average molecular weights (M_n) of C10-Th00 and C10-Th25, in which ffBT is the major dibrominated monomer in the polymerization, are lower than those of the other three polymers, indicating that the thiophene rings enhance the reactivity of the dibrominated monomer in the polymerization reaction. The actual composition of the copolymers is difficult to estimate since the difference of the theoretical mass fraction (wt%) of the characteristic elements such as F, N, and S among the polymers is too small (Table S3, Supporting Information). The solubility of the C10-Th*x* polymers decreases with increasing *x*. While C10-Th00 and C10-Th25 are soluble in both chloroform and chlorinated aromatic solvents at room temperature, the other C10-Th*x* polymers are only soluble in hot chlorinated aromatics. This difference in solubility indicates stronger aggregation of polymers in solutions by adding more thiophene rings. The thermal properties of the C10-Th*x* polymers were investigated by differential

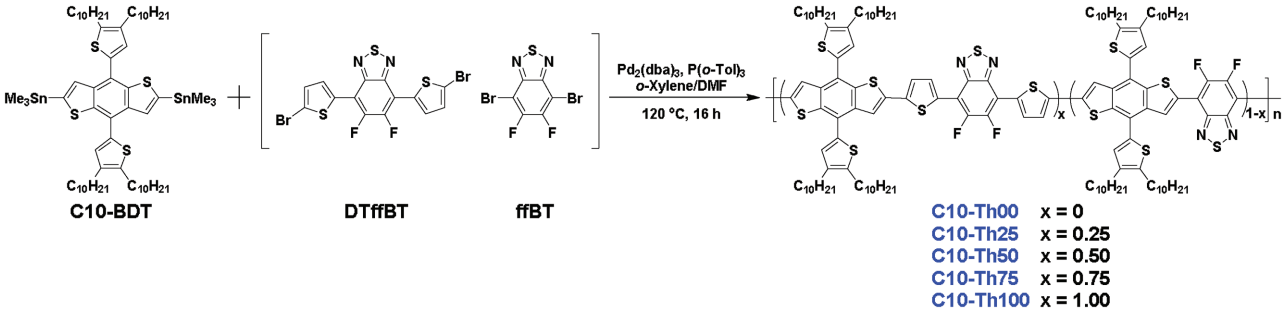

Scheme 2. Synthesis of the C10-Th*x* polymers with different percentages (*x*) of thiophene rings.

scanning calorimetry (Figure S2, Supporting Information). The C10-Th*x* polymers did not show clear melting or crystallization transitions in the scanning range from –50 to 280 °C.

2.2. Optical Properties and Energy Levels

The UV–vis absorption spectra of the five C10-Th*x* polymers in thin films (**Figure 1**a) reveal that their onsets of absorption are virtually identical and that they possess an optical band gap of E_g = 1.71–1.72 eV (Table 1). The absorption maxima do exhibit a gradual blue shift going from C10-Th00 to C10-Th100. Also the relative intensity of the first vibronic peak located at ≈610 nm increases steadily from C10-Th00 to C10-Th100. These changes confirm the gradual change of the chemical composition of the copolymers, although their actual composition may deviate from the feeding ratio of the two dibrominated monomers. The UV–vis spectra of the five C10-Th*x* polymers in *o*-DCB solution (Figure S3, Supporting Information) show similar characteristics and appear slightly blue-shifted compared to the thin films.

The frontier orbital energy levels of the polymers were determined by cyclic voltammetry experiments (Figure S4, Supporting Information). The energy levels of highest occupied molecular orbital (HOMO) and lowest unoccupied molecular orbital (LUMO) (Table 1 and Figure 1b) are reported relative to an energy level of ferrocene of –5.23 eV versus vacuum.[12] The HOMO and LUMO levels gradually move to less negative values with increasing *x* as a result of the electron-rich nature of the thiophene rings, although the differences are moderate (≤0.17 eV). Accordingly, the LUMO–LUMO offsets (ΔE_{LUMO}) and HOMO–HOMO offsets (ΔE_{HOMO}) between the C10-Th*x* polymers and [6,6]-phenyl-C_{71}-butylric acid methyl ester ([70]PCBM) increase gradually along with adding more thiophene rings into polymers. It is well recognized that larger ΔE_{LUMO} and ΔE_{HOMO} are beneficial to charge generation at donor/acceptor interface in BHJ films.[13] This influence on photocurrent of the resulting solar cells will be discussed in detail later.

2.3. Photovoltaic Properties

Photovoltaic properties of the polymers were evaluated in PSCs in a device structure of indium tin oxide (ITO)/poly(3,4-ethylen edioxythiophene):poly(styrenesulfonate)/C10-Th*x*:[70]PCBM/LiF (1 nm)/Al (100 nm) under AM1.5G illumination (100 mW cm^{-2}). The device performance of all polymers was optimized in terms of the C10-Th*x*:[70]PCBM weight ratio, solvent, and cosolvent. The thickness of the active layers is set to be ≈250 nm, which is relevant to roll-to-roll processing and close to the second interference maximum of the optical absorption for BHJ solar cells in a conventional device structure.[14] We controlled the active layer precisely to be identical with narrow limits (±5 nm) (**Table 2**). The precise control over layer thickness is important to establish reliable structure–property relationships. The current density–voltage (*J*–*V*) characteristics, external quantum efficiency (EQE) spectra, and device parameters of the optimized thick C10-Th*x*:[70]PCBM devices are shown in **Figure 2** and Table 2, and relevant device statistics are summarized in Tables S4 of the Supporting Information. The devices with an active layer thickness of ≈100 nm were also made. The data are gathered in Figure S5 and Table S5 (Supporting Information).

Figure 3 compares the open-circuit voltage (V_{oc}), short-circuit current density (J_{sc}), FF, and PCE as function of the percentage of thiophene ring (*x*). There are a few notable findings. First, the V_{oc} decreases gradually along with *x* in both sets of devices. This is consistent with the increasing HOMO energy levels of

Table 1. Molecular weights, optical properties, and energy levels of the polymers.

Polymer	M_n [kDa]	PDI	λ_{max} [nm]		E_g^{opt} [eV]	HOMO [eV]	LUMO [eV]	E_g^{CV} [eV]	ΔE_{HOMO}[a)] [eV]	ΔE_{LUMO}[b)] [eV]
			Solution	Film						
C10-Th00	33.8	3.1	664	668	1.72	–5.96	–3.75	2.21	0.49	0.52
C10-Th25	46.3	3.2	653	660	1.72	–5.88	–3.70	2.18	0.54	0.60
C10-Th50	69.4	3.7	642	654	1.71	–5.86	–3.68	2.18	0.56	0.62
C10-Th75	67.2	3.0	634	647	1.71	–5.82	–3.61	2.21	0.63	0.66
C10-Th100	65.2	2.1	631	650	1.72	–5.79	–3.58	2.21	0.66	0.69

[a)] $\Delta E_{HOMO} = E_{HOMO}$ (polymer) – E_{HOMO} ([70]PCBM); [b)] $\Delta E_{LUMO} = E_{LUMO}$ (polymer) – E_{LUMO} ([70]PCBM).

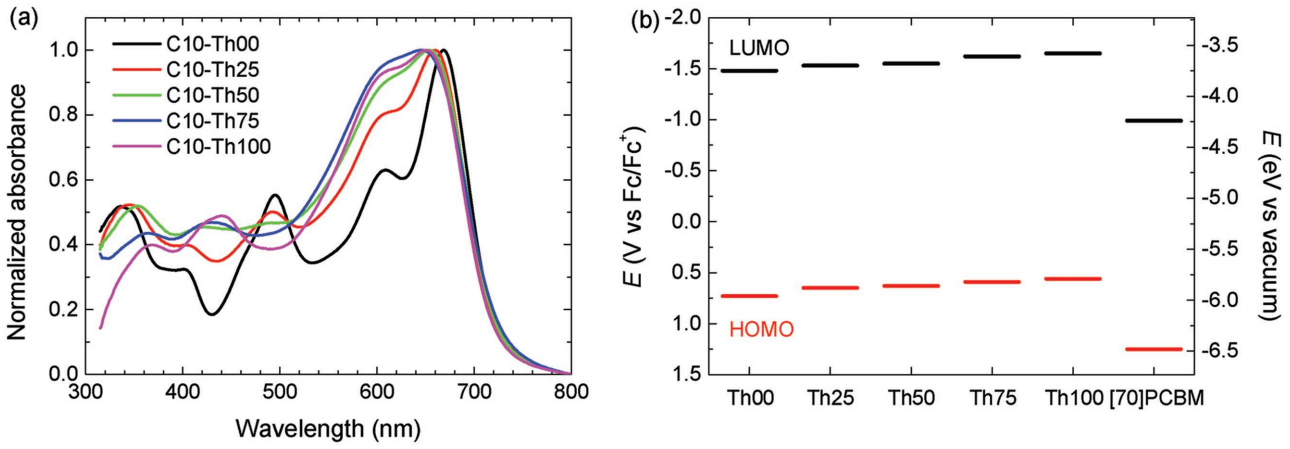

Figure 1. a) UV–vis absorption spectra of the polymers in thin films. b) Energy levels of the polymers determined by cyclic voltammetry using a work function value of –5.23 eV for Fc/Fc^+.

the polymers (Figure 1b and Table 1) and suggests that the electronic orbitals are delocalized and averaged over several repeat units even in the random copolymers C10-Th25, C10-Th50, and C10-Th75. The difference in V_{oc} between C10-Th00 and C10-Th100 is only 0.09 V. Second, there is a steady increase in J_{sc} and EQE with x; the largest step is made from C10-Th00 to C10-Th25. Similar J_{sc} and EQE enhancements upon replacing ffBT units by DTffBT units were also observed in our previous work.[5b,10,11] Third, the FF of the 250 nm devices gradually increase along with x from 0.45 to 0.61 going from C10-Th00 to C10-Th100. Synergistically, the overall PCE improves steadily, leading to an almost doubled PCE from C10-Th00 (PCE = 4.1%) to C10-Th100 (PCE = 7.7%) in thick cells. Noticeably, the gradual increase in PCE for the thick devices by introducing more thiophene rings tracks the trend of the FF very well (Figure 3b), suggesting that the FF is the dominant factor for the efficiency enhancement, although J_{sc} also play an important role in these systems.

Since the solubility of semiconducting polymers is also an important factor that influences device performance, less soluble polymers C8-Th00 and C8-Th25 with shorter side chains were also synthesized and evaluated in thick film PSCs. The device performance comparison of these two polymers with C10-Th50, C10-Th75, and C10-Th100 is presented in Figure S7 and Table S6 (Supporting Information) and reveals an identical trend of the device parameters with x.

Table 2. Performance parameters of C10-Thx:[70]PCBM solar cells with 250 nm active layer thickness.

Polymer	Thickness [nm]	J_{sc} [mA cm^{-2}]	V_{oc} [V]	FF	PCE [%]	EQE_{max}
C10-Th00	246	9.8	0.93	0.45	4.1	0.53
C10-Th25	249	12.3	0.89	0.47	5.1	0.64
C10-Th50	245	13.5	0.88	0.55	6.5	0.68
C10-Th75	240	13.9	0.84	0.56	6.5	0.69
C10-Th100	246	14.9	0.84	0.61	7.7	0.76

To understand the causes responsible for the improved PCE, J_{sc}, and FF in particular, a detailed investigation of the electrical and morphological properties was carried out.

2.4. Charge Generation, Transport, and Recombination

As mentioned above, the J_{sc} and EQE increase with x in solar cells for both thin and thick active layers. Such an increase can be ascribed to a few reasons that determine charge generation. First, the energy offsets (ΔE_{LUMO}, ΔE_{HOMO}) between the polymers and [70]PCBM increase along with the percentage of thiophene rings (x) as shown in Table 1 and Figure 1b. It is thus reasonable to speculate that the charge generation via both electron transfer from the polymer to [70]PCBM and hole transfer from [70]PCBM to the polymer at polymer:fullerene interface can be promoted by increasing x, which in turn contribute to higher EQE and J_{sc} in solar cells.[13] Second, the charge generation in these devices may be limited by exciton diffusion and exciton dissociation. To verify this hypothesis we conducted single photon counting time-resolved fluorescence experiments to estimate the exciton lifetime of the neat polymers. The transient fluorescence traces of all polymers show essentially monoexponential decay (**Figure 4**a; Table S7, Supporting Information). The exciton lifetime of C10-Th00 is ≈460 ps, and increases to ≈700 ps upon adding thiophene rings to the main chain of polymers. This suggests that a new type of exciton, with a longer lifetime, is created upon introducing the thiophene rings between the C10-BDT and ffBT units. Notably, all additional thiophene ring-containing polymers show very similar exciton lifetimes. This suggests that excitons generated in these polymers exhibit identical lifetimes because they are confined to the same repeating unit in polymer backbone. The prolonged exciton lifetime enhances the probability for excitons to reach polymer:fullerene interface, where exciton dissociation occurs. Therefore, the longer exciton lifetime for $x \geq 25\%$, contributes to an enhanced quantum yield for charge generation and, hence, a higher J_{sc}. To gain a deeper insight into the efficiency of the charge transfer processes and its correlation

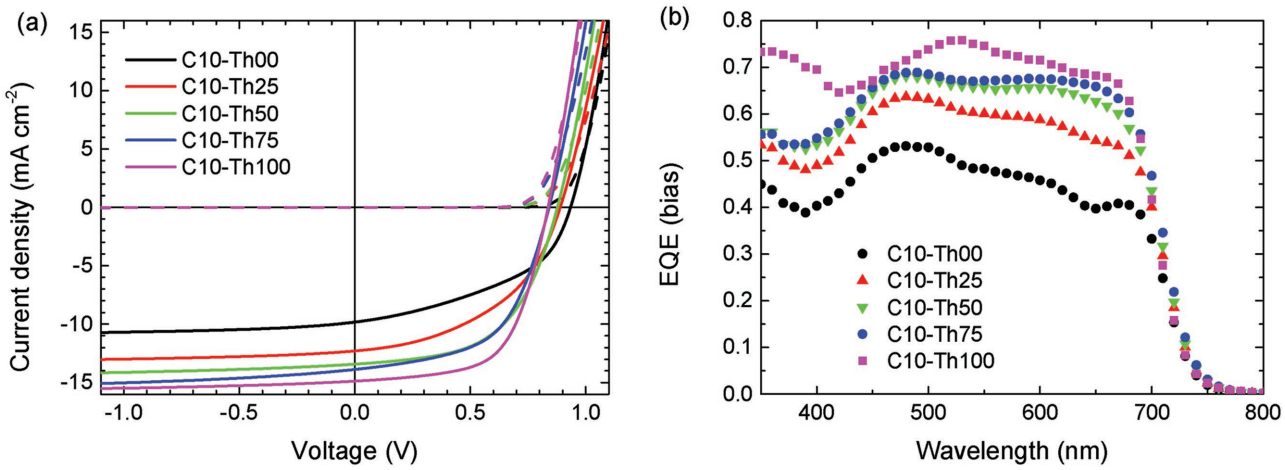

Figure 2. a) *J–V* curves and b) EQE spectra of C10-Th*x*:[70]PCBM PSCs with 250 nm active layer thickness. The different shape of the EQE spectrum of the C10-Th100 PSCs compared to the other PSCs is caused by differences in the optical field in the devices which originate from differences in ITO thickness (180 and 110 nm, respectively).[15]

with J_{sc} and EQE, the time-resolved fluorescence of the C10-Th*x*:[70]PCBM blend films were measured. We find that for each of the C10-Th*x*:[70]PCBM blends, the photoluminescence lifetime is considerably shorter than in neat polymer (Figure 4b; Table S7, Supporting Information), suggesting effective exciton quenching. The fluorescence decay of the C10-Th*x*:[70]PCBM blends can be well fitted to a biexponential decay with a fast component (τ_1) and a slow component (τ_2). The fast decay is ascribed to the charge transfer process from donor polymers to [70]PCBM and is the major decay pathway. By comparing the lifetimes in the blend and in the pure polymer, a quantum yield of the formation of charge transfer state (η_{CT}) can be extracted (Table S7, Supporting Information).[16] Figure 4c shows a plot of η_{CT} versus x in C10-Th*x*, which clearly demonstrates that charge generation is promoted upon incorporating thiophene rings into polymers. The charge generation can also be greatly influenced by the morphology of the BHJ films in addition to the exciton kinetics. The morphology analysis will be presented in detail later.

We then focused on investigating charge transport and recombination to understand the monotonic increase in FF with x in the C10-Th*x* copolymers. The hole mobility and electron mobility are often limiting factors that restrict the FF of thick-film PSCs.[7a–c,17] The hole and electron mobilities of C10-Th*x*:[70]PCBM blends were measured by space-charge-limited-current method using single carrier devices. **Figure 5**a,b shows the statistics of hole mobility and electron mobility, respectively. Going from C10-Th00 to C10-Th100, both hole and electron mobilities show a clear increasing trend. Although small on an absolute scale, any enhancement in the charge carrier mobility is beneficial to the FF, EQE, and J_{sc} in C10-Th*x*:[70]PCBM solar cells with increasing x. Nevertheless, we have the opinion that other factors are responsible for the increase in FF with x.

Therefore, bimolecular charge recombination losses were investigated, because these losses manifest themselves most substantially in the FF.[18] We investigated bimolecular recombination processes of the PSCs by analyzing the ratio between the EQE measured with light bias that affords a short-circuit current equivalent to AM1.5G illumination and the EQE measured without light bias (denoted as $\rho = EQE_{bias}/EQE_{no\ bias}$). It is worth pointing out that this measuring protocol is in principle similar to the widely used light-intensity dependency experiments.

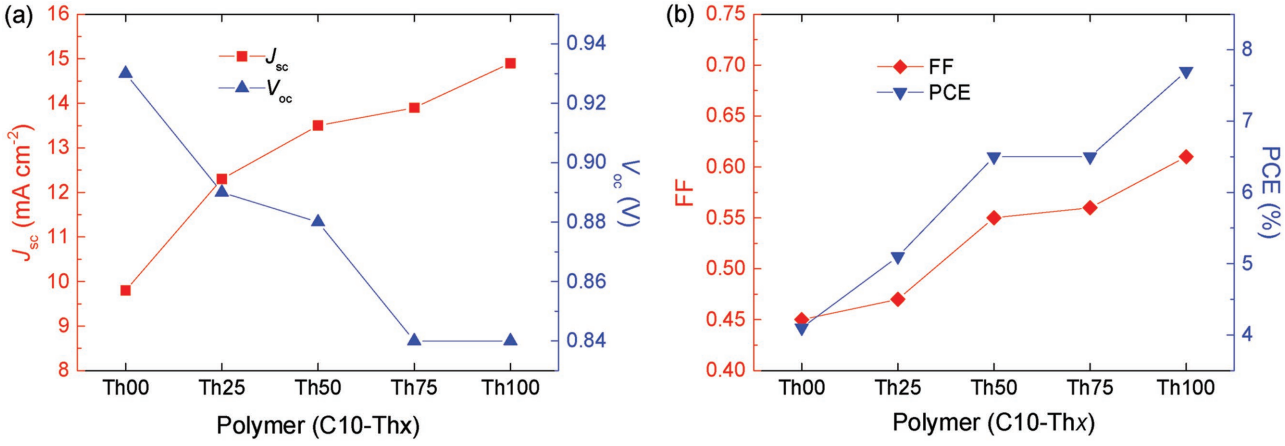

Figure 3. Change of a) J_{sc} and V_{oc} and of b) FF and PCE with x for C10-Th*x* polymers for the PSCs with 250 nm active layer thickness.

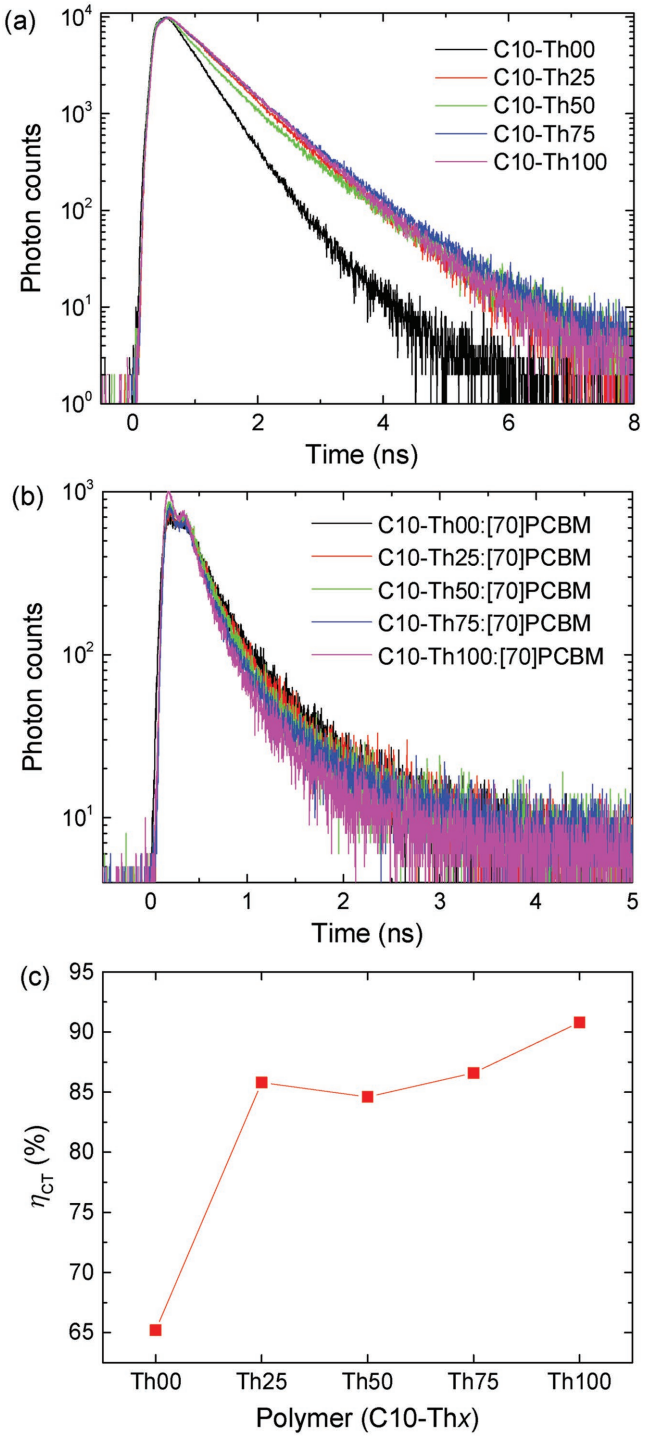

Figure 4. a,b) Time-resolved fluorescence of the pristine C10-Th*x* polymer films and C10-Th*x*:[70]PCBM blend films, respectively, recorded at 720 nm with excitation at 400 nm. c) Quantum yield of the generation of charge transfer state (η_{CT}) for the C10-Th*x*:[70]PCBM blend films.

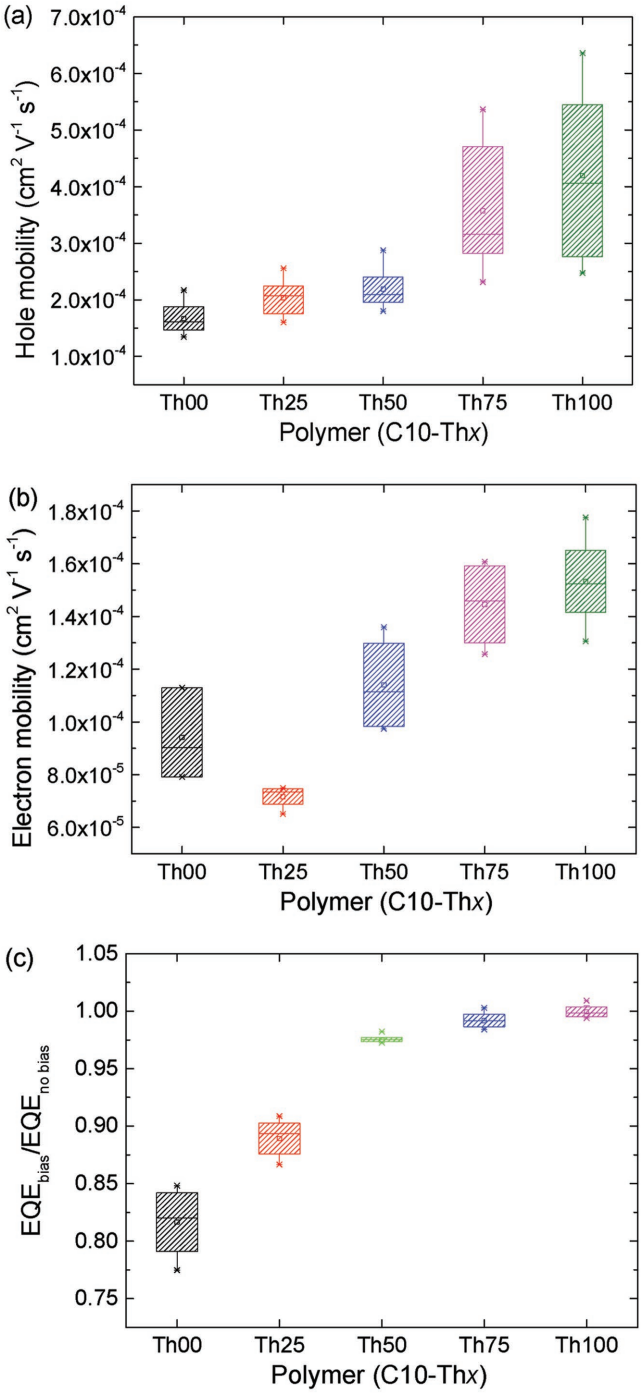

Figure 5. Charge transport and recombination of C10-Th*x*:[70]PCBM films with 250 nm layer thickness. a) Average hole mobilities in hole-only devices. b) Average electron mobilities in electron-only devices. The mobilities were estimated at an electric field of $E = 1.5 \times 10^5$ V cm^{-1}. c) Average $EQE_{bias}/EQE_{no\ bias}$ values for the solar cells.

The bimolecular recombination efficiency can be estimated from $\eta_{BR} = 1 - \rho$,[19] hence a high ρ indicates less bimolecular recombination. Figure 4c and Figure S8 (Supporting Information) shows the average ρ values in the wavelength range from 400 to 700 nm for thick (250 nm) and thin (100 nm) PSCs, respectively. The original biased and unbiased EQEs of the corresponding solar cells are provided in Figures S9 and S10 (Supporting Information). At small active layer thicknesses (100 nm) all devices show a bimolecular recombination efficiency that is less than 5% at short circuit (Figure S8,

Supporting Information), suggesting a moderate bimolecular recombination loss in these devices. However, the average ρ value reduces significantly to about 0.82 for the C10-Th00-based device at 250 nm layer thickness, consistent with the low FF. Figure 5c shows that the average ρ values gradually increase with incorporating more thiophene rings in the conjugated backbone, resulting in an average ρ of almost unity for C10-Th75 and C10-Th100. These changes in the bimolecular recombination efficiency as function of x correlate well with the variations in FF and PCE.

2.5. Polymer Ordering and BHJ Morphology

The differences in photovoltaic performance, and charge transport and recombination kinetics described above can also be related to changes in nanostructure of the polymers and BHJ morphology. The crystalline order of the polymers in both pure films and in C10-Thx:[70]PCBM blends was characterized by grazing incidence X-ray diffraction (GIXD). The results for the pure polymers and thick (250 nm) blend films are shown in **Figure 6**.

In pure films, all C10-Thx polymers adopt a face-on orientation, with the (100) diffraction corresponding to the lamellar packing appearing in the in-plane direction and the π-stacking peak in the out-of-plane direction. It is quite clear in Figure 6b that C10-Th00 has a much sharper (100) diffraction peak in the in-plane direction, and thus a stronger alkyl-to-alkyl interaction in solid state, than the other polymers. Introducing thiophene rings not only affects the (100) diffraction, but also the π-stacking in the out-of-plane direction, as seen from the change of π-stacking peaks. In BHJ blends, this trend is preserved. Yet the π-stacking becomes less obvious since the [70]PCBM diffractions (≈1.3 and ≈1.9 Å^{-1}) overlap with π-stacking peak. Detailed crystalline information regarding alkyl-to-alkyl interaction and π-stacking in pure film is obtained by fitting the diffraction profiles, and related results are shown in **Figure 7** and **Table 3**. It is quite interesting that adding thiophene rings affects the crystalline packing in two dimensions. As seen from Figure 7a, the lamellar (100) distances decrease progressively with increasing the content of thiophene ring, along with a continuous reduction in (100) crystal coherence length (or crystal size). Thus introducing thiophene ring in this direction perturbs the chain regularity, reducing the lamellar order in the film. The reduced distance in (100) spacing in the C10-Th100 polymer compared to the C10-Th00 polymer is quite large. This is expected since more space in-between alkyl chains leads to tighter packing, as chains have more organizational freedom. The thiophene rings also affect the π-stacking, which is orthogonal to alkyl–alkyl interdigitation. As seen from Figure 7b, C10-Th00 has a π-stacking distance of 0.365 nm and a crystal coherence length of 2.2 nm. Introducing thiophene rings leads to reduction in crystal size. In C10-Th25 sample, the π-stacking distance increased to 0.369 nm. Thus adding 25% of thiophene rings leads to main chain disorder in both the (100) and π-stacking directions. Further addition of thiophene rings should have the similar effect. However, the more alkyl chain free space added by thiophene rings counteracts the structure disorder, and thus π-stacking distance reduces. In C10-Th100 polymer, regained regularity and larger chain

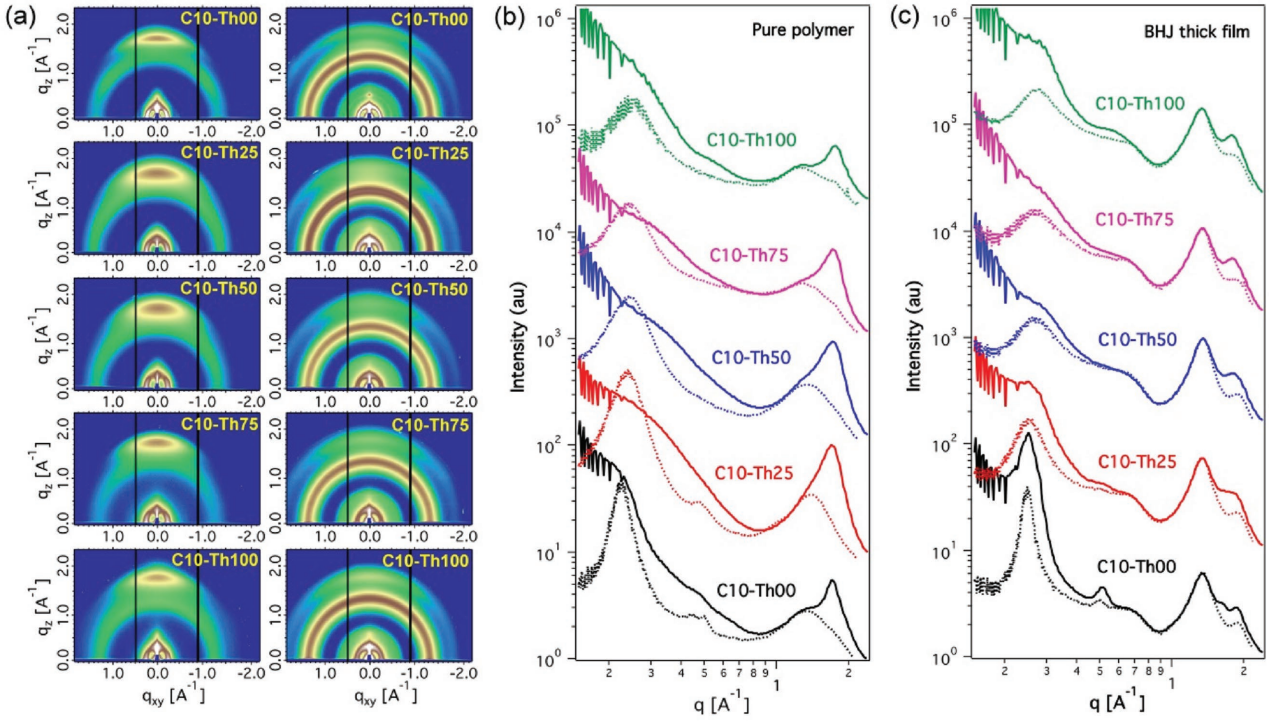

Figure 6. GIXD of pure polymers and thick (≈250 nm) BHJ films. a) Diffraction patterns (left: pure polymers; right: BHJ blends). b) Pure polymer line-cut profiles. c) BHJ film line-cut profiles (solid line: out-of-plane line-cut profiles; dotted line: in-plane line-cut profiles).

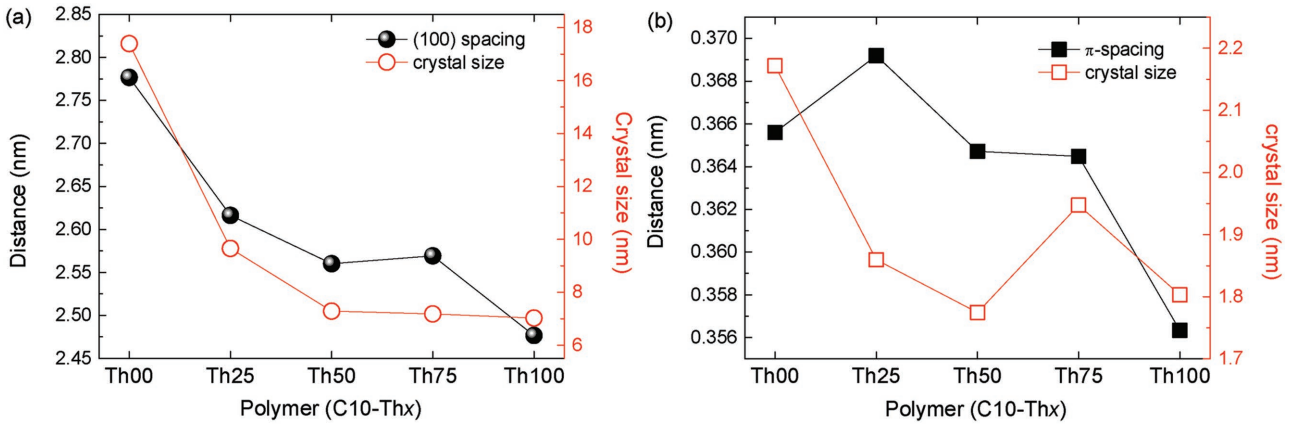

Figure 7. GIXD fitting analysis of a) (100) crystal packing distance and coherence length, and b) π-stacking crystal packing distance and coherence length for pure C10-Th*x* films.

free space improved the packing order, a 0.356 nm π-stacking distance is recorded. The improved π-stacking should help with charge transport and device performances, as seen in PSC and electrical characterizations.

The morphology of the C10-Th*x*:[70]PCBM blends was further investigated by transmission electron microscopy (TEM) and resonant soft X-ray scattering (RSoXS). The results for the thick films (≈250 nm) are shown in **Figure 8** and **9**. Figure 8 reveals that the film of the C10-Th00:[70]PCBM blend shows a clear phase separation with relatively large domain sizes. The dark regions are [70]PCBM-rich domains and the brighter fibrillar structures are rich in C10-Th00. With this phase-separated morphology, the low J_{sc} and EQE are likely due to a diminished polymer/fullerene interface for charge generation. The FF in thin films (≈100 nm) is still high with such a suboptimal morphology (Figure S11, Supporting Information), because the domain size in this phase-separated structure is commensurate with film thickness. Even though [70]PCBM aggregated, the transport pathway is unblocked. At higher thickness (≈250 nm), the domain connectivity is an issue that leads to reduced mobility and thus a low FF. From C10-Th25 to C10-Th100, the films show more finely dispersed fibrillary nanostructures and bicontinuous networks. This morphology is seen in many high performance PSC blends that provide good current output and FF.

More structural details are obtained from RSoXS experiments (Figure 9). The C10-Th00:[70]PCBM blend shows a broad scattering peak at ≈0.0035 Å^{-1}, giving a length scale of phase separation of 182 nm. This length scale correlates well with [70]PCBM aggregation spacing. This scattering feature diminishes the fibril network that is hided in high q scattering region. Such a large phase separation leads to low J_{sc} as seen from device characterization. Adding 25% of thiophene rings leads to drastic change in the BHJ morphology as seen in Figure 8. Correspondingly, the scattering intensity largely reduced and a broad hump shows up to ≈0.0088 Å^{-1}, giving a typical distance of 71 nm. Thus introducing thiophene rings leads to a more favorable donor–acceptor interaction, and larger sized [70]PCBM aggregation is suppressed. This broad scattering should be comprised of reduced [70]PCBM aggregations and polymer fibril networks, which cannot be fully resolved and separated by both TEM and RSoXS. Further adding thiophene rings to 50% (C10-Th50) leads to an even more homogeneous mixture, as seen from reduced scattering intensity. A scattering hump at ≈0.012 Å^{-1} is seen, corresponding to a distance of 52 nm. Adding 75% and 100% of thiophene rings does not further reduce the length scale of phase separation but continuously reduces scattering intensity (seen from thickness normalized RSoXS results). Thus changing from C10-Th00 to C10-Th100, the material interaction in BHJ blends shows a monotonic trend that favors intermixing, leading to a fibril network dominated morphology. The C10-Th100 BHJ blends shows a better-defined scattering peak around 0.012 Å^{-1} (52 nm), and RSoXS scattering in extreme low q region (<0.003 Å^{-1}) is the lowest in intensity. Thus this BHJ film is more uniform globally and a better-defined fibril network morphology is expected.

Table 3. Structure features of C10-Th*x* in pure films and characteristic length scale of phase separation in blend films of ≈250 nm thickness.

Polymer	Lamellar		π-Stacking		Domain spacing [nm]
	(100) distance [nm]	Coherence length [nm]	π–π distance [nm]	Coherence length [nm]	
C10-Th00	2.78	17.39	0.366	2.17	182
C10-Th25	2.62	9.66	0.369	1.86	71
C10-Th50	2.56	7.29	0.365	1.77	52
C10-Th75	2.57	7.18	0.364	1.95	52
C10-Th100	2.48	7.02	0.356	1.80	52

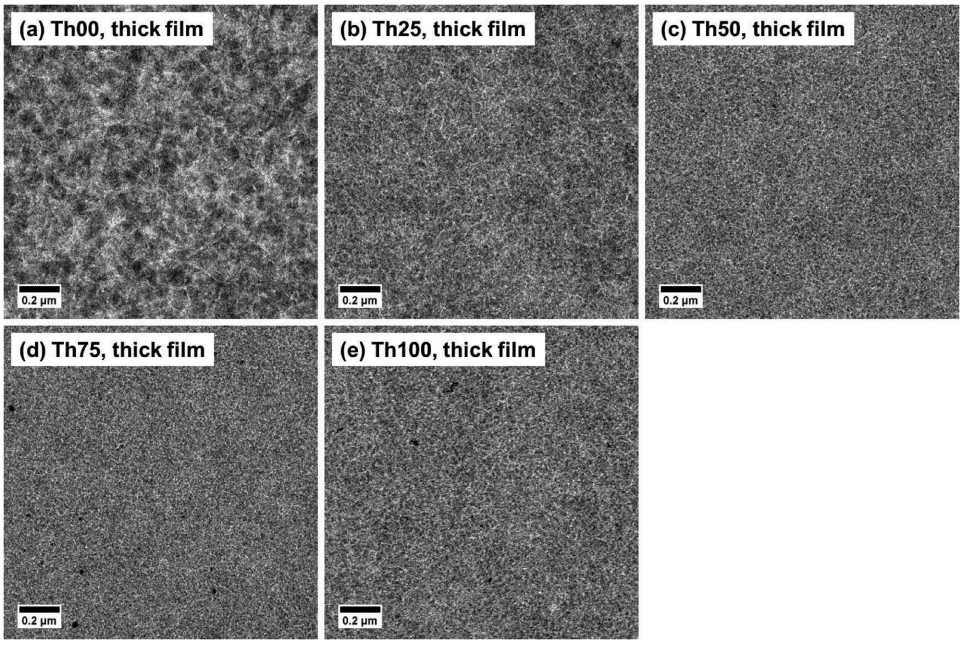

Figure 8. Bright-field TEM images of C10-Thx:[70]PCBM blend films at ≈250 nm thickness formed under the same conditions as solar cell fabrications for a) C10-Th00, b) C10-Th25, c) C10-Th50, d) C10-Th75, and e) C10-Th100. Image size: 1.5 × 1.5 μm^2; scale bar: 0.2 μm.

The (100) crystal size calculated from GIXD characterization is ≈7 nm, which corresponds to the fibril width in TEM. A 1:1.5 donor:acceptor blending ratio for C10-Th100 is used in device fabrication, besides, polymer donor has considerable amount of amorphous content. Thus the 52 nm spacing corresponding to the fibril-to-fibril spacing in BHJ blends. From these results it appears that in this series of material blends, the reduced length scale of phase separation gives rise to enhanced J_{sc} in PSC devices. In the champion device of C10-Th100:PCBM, with the best J_{sc} and FF, the more uniform and better defined morphology allows a more effective dissociation of excitons and collection of formed charges from both donor and acceptor domains.

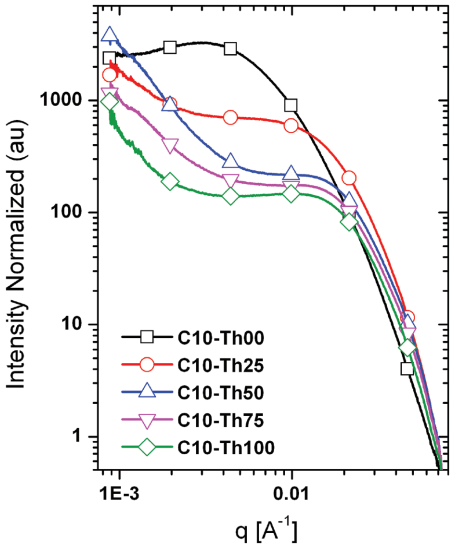

Figure 9. RSoXS of thick (≈250 nm) BHJ films based on C10-Thx:[70]PCBM.

3. Conclusion

In conclusion, a set of C10-Th*x* conjugated polymers based on benzo[1,2-*b*:4,5-*b*′]dithiophene and 5,6-difluorobenzo[2,1,3]-thiazole with a systematic increase of thiophene rings in the polymer main chain were designed and synthesized. Interestingly, for thick photoactive layers based on these materials there is a monotonic relation between the relative number *x* of thiophene rings in the conjugated polymer main chain and fill factor, which is a dominant factor that determines the performance of PSCs. The steady increase of fill factor results in a rising overall efficiency with increasing content of thiophene rings. A detailed investigation revealed that the "thiophene ring effect" is a combined result of an enhanced charge mobility and a suppressed bimolecular charge recombination, which we attribute to a more favorable polymer chain packing and a finer phase separation. The rationale behind the beneficial effect is that the additional unsubstituted thiophene rings allow for a reduced π-stacking distance and a reduced lamellar distance which improve charge transport, and reduce the solubility of the polymer chain which results in finer phase separation in blends with fullerenes.[20] Our results allow to rationalize the remarkable role of thiophene rings as an indispensable element to maintain a high efficiency also for thick-film polymer solar cells. Our discovery provides an explicit guideline for designing and developing practical useful polymers for application in PSCs in future,[17,21] where a low sensitivity to thickness variations is an important advantage in manufacturing. Moreover, the correlations between molecular structure and

fill factor observed in this paper are a motivation to search for methods that can enhance charge carrier mobility, suppress charge recombination, tune polymer packing, and optimize morphology to achieve high PCE at large active layer thickness, which in turn favors large-scale processing and multijunction PSCs.

Supporting Information

Supporting Information is available from the Wiley Online Library or from the author.

Acknowledgements

C.D. and K.G. contributed equally to this work. The authors thank Ralf Bovee and Gaël Heintges for GPC analysis. The work was performed in the framework of the Mujulima project that received funding from the European Commission's Seventh Framework Programme (Grant Agreement No. 604148). The research leading to these results had also received funding from the European Research Council under the European Union's Seventh Framework Programme (FP/2007-2013)/ERC Grant Agreement No. 339031. This research was the part of the Solliance OPV program and received funding from the Ministry of Education, Culture and Science (Gravity program 024.001.035). Portions of this research were carried out at beamline 7.3.3 and 11.0.1.2 at the Advanced Light Source, Molecular Foundry, and National Center for Electron Micoscopy, Lawrence Berkeley National Laboratory, which was supported by the DOE, Office of Science, and Office of Basic Energy Sciences.

Conflict of Interest

The authors declare no conflict of interest.

Keywords

active layer, fill factor, polymer solar cells, thick film, thiophene ring

Received: February 26, 2017
Revised: April 1, 2017
Published online: July 10, 2017

[1] a) G. Yu, J. Gao, J. C. Hummelen, F. Wudl, A. J. Heeger, *Science* **1995**, *270*, 1789; b) L. Lu, T. Zheng, Q. Wu, A. M. Schneider, D. Zhao, L. Yu, *Chem. Rev.* **2015**, *115*, 12666.

[2] a) C.-C. Chen, W.-H. Chang, K. Yoshimura, K. Ohya, J. You, J. Gao, Z. Hong, Y. Yang, *Adv. Mater.* **2014**, *26*, 5670; b) A. R. b. M. Yusoff, D. Kim, H. P. Kim, F. K. Shneider, W. J. da Silva, J. Jang, *Energy Environ. Sci.* **2015**, *8*, 303; c) J. Zhao, Y. Li, G. Yang, K. Jiang, H. Lin, H. Ade, W. Ma, H. Yan, *Nature Energy* **2016**, *1*, 15027; d) K. Zhang, K. Gao, R. Xia, Z. Wu, C. Sun, J. Cao, L. Qian, W. Li, S. Liu, F. Huang, X. Peng, L. Ding, H.-L. Yip, Y. Cao, *Adv. Mater.* **2016**, *28*, 4817; e) Z. Zheng, S. Zhang, J. Zhang, Y. Qin, W. Li, R. Yu, Z. Wei, J. Hou, *Adv. Mater.* **2016**, *28*, 5133.

[3] a) C. H. Peters, I. T. Sachs-Quintana, J. P. Kastrop, S. Beaupré, M. Leclerc, M. D. McGehee, *Adv. Energy Mater.* **2011**, *1*, 491; b) M. Jørgensen, K. Norrman, S. A. Gevorgyan, T. Tromholt, B. Andreasen, F. C. Krebs, *Adv. Mater.* **2012**, *24*, 580.

[4] a) A. Armin, M. Hambsch, P. Wolfer, H. Jin, J. Li, Z. Shi, P. L. Burn, P. Meredith, *Adv. Energy Mater.* **2015**, *5*, 1401221; b) R. Po, A. Bernardi, A. Calabrese, C. Carbonera, G. Corso, A. Pellegrino, *Energy Environ. Sci.* **2014**, *7*, 925; c) K. Zhang, Z. Hu, C. Sun, Z. Wu, F. Huang, Y. Cao, *Chem. Mater.* **2017**, *29*, 141.

[5] a) T. Ameri, G. Dennler, C. Lungenschmied, C. J. Brabec, *Energy Environ. Sci.* **2009**, *2*, 347; b) C. Duan, A. Furlan, J. J. van Franeker, R. E. M. Willems, M. M. Wienk, R. A. J. Janssen, *Adv. Mater.* **2015**, *27*, 4461.

[6] a) Z. C. He, C. M. Zhong, S. J. Su, M. Xu, H. B. Wu, Y. Cao, *Nat. Photonics* **2012**, *6*, 591; b) Z. He, B. Xiao, F. Liu, H. Wu, Y. Yang, S. Xiao, C. Wang, T. P. Russell, Y. Cao, *Nat. Photonics* **2015**, *9*, 174.

[7] a) P. W. M. Blom, V. D. Mihailetchi, L. J. A. Koster, D. E. Markov, *Adv. Mater.* **2007**, *19*, 1551; b) T. Kirchartz, T. Agostinelli, M. Campoy-Quiles, W. Gong, J. Nelson, *J. Phys. Chem. Lett.* **2012**, *3*, 3470; c) J. A. Bartelt, D. Lam, T. M. Burke, S. M. Sweetnam, M. D. McGehee, *Adv. Energy Mater.* **2015**, *5*, 1500577; d) A. Armin, A. Yazmaciyan, M. Hambsch, J. Li, P. L. Burn, P. Meredith, *ACS Photonics* **2015**, *2*, 1745.

[8] a) C. Duan, F. Huang, Y. Cao, *Polym. Chem.* **2015**, *6*, 8081; b) W. Li, K. H. Hendriks, W. S. C. Roelofs, Y. Kim, M. M. Wienk, R. A. J. Janssen, *Adv. Mater.* **2013**, *25*, 3182; c) H. Choi, S.-J. Ko, T. Kim, P.-O. Morin, B. Walker, B. H. Lee, M. Leclerc, J. Y. Kim, A. J. Heeger, *Adv. Mater.* **2015**, *27*, 3318; d) S. C. Price, A. C. Stuart, L. Q. Yang, H. X. Zhou, W. You, *J. Am. Chem. Soc.* **2011**, *133*, 4625; e) T. Yang, M. Wang, C. Duan, X. Hu, L. Huang, J. Peng, F. Huang, X. Gong, *Energy Environ. Sci.* **2012**, *5*, 8208; f) Z. Chen, P. Cai, J. Chen, X. Liu, L. Zhang, L. Lan, J. Peng, Y. Ma, Y. Cao, *Adv. Mater.* **2014**, *26*, 2586; g) T. L. Nguyen, H. Choi, S. J. Ko, M. A. Uddin, B. Walker, S. Yum, J. E. Jeong, M. H. Yun, T. J. Shin, S. Hwang, J. Y. Kim, H. Y. Woo, *Energy Environ. Sci.* **2014**, *7*, 3040; h) Y. Liu, J. Zhao, Z. Li, C. Mu, W. Ma, H. Hu, K. Jiang, H. Lin, H. Ade, H. Yan, *Nat. Commun.* **2014**, *5*, 5293; i) Z. Li, H. Lin, K. Jiang, J. Carpenter, Y. Li, Y. Liu, H. Hu, J. Zhao, W. Ma, H. Ade, H. Yan, *Nano Energy* **2015**, *15*, 607; j) H. Hu, K. Jiang, G. Yang, J. Liu, Z. Li, H. Lin, Y. Liu, J. Zhao, J. Zhang, F. Huang, Y. Qu, W. Ma, H. Yan, *J. Am. Chem. Soc.* **2015**, *137*, 14149; k) J. Zhao, Y. Li, A. Hunt, J. Zhang, H. Yao, Z. Li, J. Zhang, F. Huang, H. Ade, H. Yan, *Adv. Mater.* **2016**, *28*, 1868; l) X. Hu, C. Yi, M. Wang, C.-H. Hsu, S. Liu, K. Zhang, C. Zhong, F. Huang, X. Gong, Y. Cao, *Adv. Energy Mater.* **2014**, *4*, 1400378; m) V. Vohra, K. Kawashima, T. Kakara, T. Koganezawa, I. Osaka, K. Takimiya, H. Murata, *Nat. Photonics* **2015**, *9*, 403; n) K. Kawashima, T. Fukuhara, Y. Suda, Y. Suzuki, T. Koganezawa, H. Yoshida, H. Ohkita, I. Osaka, K. Takimiya, *J. Am. Chem. Soc.* **2016**, *138*, 10265; o) Y. Jin, Z. Chen, S. Dong, N. Zheng, L. Ying, X.-F. Jiang, F. Liu, F. Huang, Y. Cao, *Adv. Mater.* **2016**, *28*, 9811; p) Q. Fan, W. Su, X. Guo, B. Guo, W. Li, Y. Zhang, K. Wang, M. Zhang, Y. Li, *Adv. Energy Mater.* **2016**, *6*, 1600430.

[9] a) J. Huang, J. H. Carpenter, C.-Z. Li, J.-S. Yu, H. Ade, A. K. Y. Jen, *Adv. Mater.* **2016**, *28*, 967; b) J. Chen, L. Zhang, X. Jiang, K. Gao, F. Liu, X. Gong, J. Chen, Y. Cao, *Adv. Energy Mater.* **2017**, *7*, 1601344.

[10] C. Duan, R. E. M. Willems, J. J. van Franeker, B. J. Bruijnaers, M. M. Wienk, R. A. J. Janssen, *J. Mater. Chem. A* **2016**, *4*, 1855.

[11] C. Duan, K. Gao, J. J. van Franeker, F. Liu, M. M. Wienk, R. A. J. Janssen, *J. Am. Chem. Soc.* **2016**, *138*, 10782.

[12] D. Veldman, S. C. J. Meskers, R. A. J. Janssen, *Adv. Funct. Mater.* **2009**, *19*, 1939.

[13] a) L. J. A. Koster, V. D. Mihailetchi, P. W. M. Blom, *Appl. Phys. Lett.* **2006**, *88*, 093511; b) K. H. Hendriks, A. S. G. Wijpkema,

J. J. van Franeker, M. M. Wienk, R. A. J. Janssen, *J. Am. Chem. Soc.* **2016**, *138*, 10026.
[14] G. Dennler, M. C. Scharber, C. J. Brabec, *Adv. Mater.* **2009**, *21*, 1323.
[15] P. Doggart, N. Bristow, J. Kettle, *J. Appl. Phys.* **2014**, *116*, 103103.
[16] J. Lakowicz, *Principles of Fluorescence Spectroscopy*, Springer Science + Business Media, New York **2006**.
[17] W. Li, S. Albrecht, L. Yang, S. Roland, J. R. Tumbleston, T. McAfee, L. Yan, M. A. Kelly, H. Ade, D. Neher, W. You, *J. Am. Chem. Soc.* **2014**, *136*, 15566.
[18] C. G. Shuttle, R. Hamilton, B. C. O'Regan, J. Nelson, J. R. Durrant, *Proc. Natl. Acad. Sci. USA* **2010**, *107*, 16448.
[19] L. J. A. Koster, M. Kemerink, M. M. Wienk, K. Maturová, R. A. J. Janssen, *Adv. Mater.* **2011**, *23*, 1670.
[20] J. J. van Franeker, G. H. L. Heintges, C. Schaefer, G. Portale, W. Li, M. M. Wienk, P. van der Schoot, R. A. J. Janssen, *J. Am. Chem. Soc.* **2015**, *137*, 11783.
[21] J. Gao, L. Dou, W. Chen, C.-C. Chen, X. Guo, J. You, B. Bob, W.-H. Chang, J. Strzalka, C. Wang, G. Li, Y. Yang, *Adv. Energy Mater.* **2014**, *4*, 1300739.